



A vertical representation of soil carbon in the JULES land surface scheme (vn4.3_permafrost) with a focus on permafrost regions

Eleanor J. Burke¹, Sarah E. Chadburn^{2,3}, and Altug Ekici^{2,4}

¹Met Office Hadley Centre, Fitzroy Road, Exeter, EX1 3PB, UK

²University of Exeter, College of Engineering, Mathematics and Physical Sciences, Exeter, EX4 4QF, UK

³University of Leeds, School of Earth and Environment, Leeds, LS2 9JT, UK

⁴Uni Research Climate and Bjerknes Centre for Climate Research, Bergen, Norway

Correspondence to: Eleanor J. Burke (eleanor.burke@metoffice.gov.uk)

Received: 5 September 2016 – Discussion started: 28 September 2016

Revised: 16 January 2017 – Accepted: 19 January 2017 – Published: 24 February 2017

Abstract. An improved representation of the carbon cycle in permafrost regions will enable more realistic projections of the future climate–carbon system. Currently JULES (the Joint UK Land Environment Simulator) – the land surface model of the UK Earth System Model (UKESM) – uses the standard four-pool RothC soil carbon model. This paper describes a new version of JULES (vn4.3_permafrost) in which the soil vertical dimension is added to the soil carbon model, with a set of four pools in every soil layer. The respiration rate in each soil layer depends on the temperature and moisture conditions in that layer. Cryoturbation/bioturbation processes, which transfer soil carbon between layers, are represented by diffusive mixing. The litter inputs and the soil respiration are both parametrized to decrease with increasing depth. The model now includes a tracer so that selected soil carbon can be labelled and tracked through a simulation. Simulations show an improvement in the large-scale horizontal and vertical distribution of soil carbon over the standard version of JULES (vn4.3). Like the standard version of JULES, the vertically discretized model is still unable to simulate enough soil carbon in the tundra regions. This is in part because JULES underestimates the plant productivity over the tundra, but also because not all of the processes relevant for the accumulation of permafrost carbon, such as peat development, are included in the model. In comparison with the standard model, the vertically discretized model shows a delay in the onset of soil respiration in the spring, resulting in an increased net uptake of carbon during this time. In order to provide a more suitable representation of permafrost carbon for quantifying the permafrost

carbon feedback within UKESM, the deep soil carbon in the permafrost region (below 1 m) was initialized using the observed soil carbon. There is now a slight drift in the soil carbon ($< 0.018\% \text{ decade}^{-1}$), but the change in simulated soil carbon over the 20th century, when there is little climate change, is comparable to the original vertically discretized model and significantly larger than the drift.

1 Introduction

Soils contain the largest terrestrial carbon store, estimated at around 2000 Pg in the top 2 m of soil (Batjes, 2016; Shang-guan et al., 2014). In particular, permafrost regions contain a large amount of soil carbon, much of which is old carbon that is prevented from decomposing due to the frozen conditions (Schirrmeister et al., 2002; Zimov et al., 2006; Smith et al., 2004). The most recent estimate suggests that there is approximately 1035 Pg carbon in the top 3 m of permafrost soil, and another 272 Pg carbon below 3 m in e.g. yedoma deposits (Hugelius et al., 2014). This relatively inert carbon has a critical role to play in the terrestrial feedbacks to climate change, as it decomposes when permafrost thaws, releasing greenhouse gases to the atmosphere and amplifying climate warming (Schaefer et al., 2014; Schuur et al., 2015; MacDougall et al., 2012; Burke et al., 2012, 2013; Schneider von Deimling et al., 2012, 2015). Current estimates suggest that there will be 35–205 Pg of permafrost carbon emissions by 2100 (Schuur et al., 2015; Schaefer et al., 2014). However, the magnitude and timing of carbon fluxes caused by per-

mafrost degradation remain highly uncertain, partly because of incomplete observations and partly because modelling of many of the relevant processes is still in its infancy.

Earth system models (ESMs) play an important role in understanding feedbacks and global impacts – aiming to include all significant links between different components of the Earth system. There is currently a considerable uncertainty in the soil carbon cycle feedbacks, and size and response of soil carbon pools to a changing climate in ESM simulations. For example in the CMIP5 models the soil carbon stocks correlate poorly with observations (Todd-Brown et al., 2013; Anav et al., 2013), which is very likely due to missing processes in the models (Todd-Brown et al., 2013). This in turn impacts the sensitivity of soil organic matter to environmental change, leading, for example, to the wide range of estimates of permafrost carbon emissions under future warming (Schuur et al., 2015). Only a few studies have explicitly included permafrost carbon coupled with the climate in an ESM, e.g. MacDougall et al. (2012) and MacDougall and Knutti (2016).

Recent developments in permafrost physics such as including soil freezing, organic soil properties, improved snow schemes, more realistic soil depths and physical impacts of mosses and lichens (Gouttevin et al., 2012; Lawrence et al., 2008; Ekici et al., 2014; Paquin and Sushama, 2015; Chadburn et al., 2015a, b; Porada et al., 2016) mean that the rate of permafrost thaw is now more realistic in many of the land surface components of ESMs. Adding a vertical representation of soil carbon is now required to enable a representation of permafrost carbon in ESMs (Tian et al., 2015). Without a vertical representation, decomposition rates are determined only by soil temperatures above the maximum summer thaw depth, so the very slow turnover of deep carbon in the permanently frozen soil is not represented. Vertically resolved soil carbon and nitrogen have recently been introduced into the land surface schemes from several ESMs (Koven et al., 2013, 2009; Jafarov and Schaefer, 2016; MacDougall et al., 2012), some of which will participate in CMIP6. Other vertically resolved soil carbon models have been applied on a site scale (Herbst et al., 2008; Braakhekke et al., 2011), with a view to being included in ESMs in future. It should be noted that any model that is included in an ESM must be applicable globally as well as for permafrost regions.

Typically soil carbon within an ESM is “spun-up” using pre-industrial climate until the soil carbon is relatively stable between spin-up iterations. However, models are often missing many relevant burial processes such as alluvial sedimentation; dust deposition; peat development and cryoturbation (Schuur et al., 2008; Dutta et al., 2006; Ping et al., 2015). Therefore there will be biases in the soil carbon which will impact projections of permafrost carbon emissions (Foeroid et al., 2012). One method of reducing these biases is to initialize the soil organic carbon stocks using the observed soil carbon distribution (Schneider von Deimling et al., 2015; Jafarov and Schaefer, 2016). However, this may result in a sig-

nificant drift back towards the equilibrium state, and thus it is important to check that this drift is not so large as to mask the climate signal.

The purpose of this paper is to describe and evaluate a new vertically resolved soil carbon scheme integrated within the Joint UK Land-Environment Simulator (JULES at vn4.3_permafrost), which is the land surface component of the UK Earth System Model (UKESM). We describe the model structure and evaluate the results of global simulations over the 20th century against observations of soil carbon stocks and respiration fluxes. The results are also compared with the original standard zero-layer soil carbon scheme. Although the ability of the vertically discretized soil carbon model to represent the distribution of soil carbon is globally relevant, the current assessment focuses particularly on permafrost regions.

2 Materials and methods

2.1 JULES model description

JULES is the land surface component of the new community ESM, UKESM (Jones and Sellar, 2015). It can also be run offline forced by observed meteorology at a regional or point scale as well as globally. JULES is described in Best et al. (2011) and Clark et al. (2011). It is a community model with many users and ongoing developments. For recent developments see, for example, Harper et al. (2016) and Chadburn et al. (2015a).

JULES includes a dynamic vegetation model (TRIFFID), surface energy balance, a dynamic snowpack model (one dimensional), vertical heat and water fluxes, soil freezing, large scale hydrology, and carbon fluxes and storage in both vegetation and soil. It also includes specific representations of crops, urban heat and water dynamics, fire diagnostics and river routing.

2.2 Model developments

2.2.1 RothC soil carbon model

The standard soil carbon model in JULES is based on RothC (Jenkinson et al., 1990; Jenkinson and Coleman, 1999), and described in detail in Clark et al. (2011). There are four pools: decomposable plant material (DPM), resistant plant material (RPM), microbial biomass (BIO), and hummus (HUM). The soil carbon dynamics are represented as follows:

$$\frac{dC_{DPM}}{dt} = f_{dpm}\Lambda_c - R_{DPM}, \quad (1)$$

$$\frac{dC_{RPM}}{dt} = (1 - f_{dpm})\Lambda_c - R_{RPM}, \quad (2)$$

$$\frac{dC_{BIO}}{dt} = 0.46\beta_R R_{tot} - R_{BIO}, \quad (3)$$

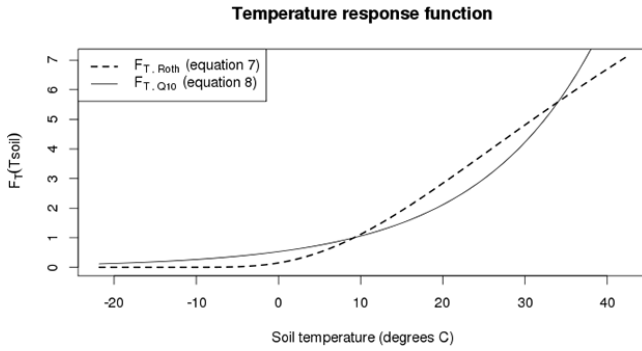


Figure 1. The temperature response curves [$F_T(T_{\text{soil}})$] from Eqs. (7) and (6).

$$\frac{dC_{\text{HUM}}}{dt} = 0.54\beta_R R_{\text{tot}} - R_{\text{HUM}}, \quad (4)$$

where $R_{\text{tot}} = R_{\text{DPM}} + R_{\text{RPM}} + R_{\text{BIO}} + R_{\text{HUM}}$ is the total respiration in $\text{kg C m}^{-2} \text{s}^{-1}$, t is the time in s, the C_i are the carbon pools in kg C m^{-2} , f_{dpm} is the fraction of litter that goes into DPM (dependent on vegetation type), Λ_c is the total litter input in $\text{kg C m}^{-2} \text{s}^{-1}$, and β_R is the fraction of soil respiration which is emitted to the atmosphere. This depends on soil texture.

The respiration for each pool (R_i , where i is one of (DPM, RPM, BIO, HUM)) is given by:

$$R_i = k_i C_i F_T(T_{\text{soil}}) F_s(s) F_v(v), \quad (5)$$

where the k_i are fixed constants in s^{-1} (Clark et al., 2011). The functions of temperature [$F_T(T_{\text{soil}})$] and moisture [$F_s(s)$] depend on the temperature and moisture content near the surface. The function for vegetation $F_v(v)$ is a function of the vegetation cover.

There are two different functions available to represent the impact of temperature on soil respiration. The first option for the temperature function, $F_{T,Q10}$ (Eq. 6), is a commonly used exponential function, and the second option, $F_{T,Roth}$ (Eq. 7), is based on the function from the original RothC model:

$$F_{T,Q10}(T_{\text{soil}}) = Q_{10}^{(T_{\text{soil}} - 298.15)/10}, \quad (6)$$

$$F_{T,Roth}(T_{\text{soil}}) = \frac{47.9}{1 + e^{106/(T_{\text{soil}} - 254.85)}}, \quad (7)$$

where T_{soil} is the soil temperature in K and $Q_{10} = 2$. Figure 1 shows that $F_{T,Q10}$ allows much more respiration at temperatures below freezing than $F_{T,Roth}$.

The moisture function in the current version of JULES (vn4.3) is parametrized as

$$F_s(s) = \begin{cases} 1 - 0.8(s - s_0) & ; \quad s > s_0 \\ 0.2 + 0.8 \left(\frac{s - s_{\text{min}}}{s_0 - s_{\text{min}}} \right) & ; \quad s_{\text{min}} < s \leq s_0 \\ 0.2 & ; \quad s \leq s_{\text{min}} \end{cases}, \quad (8)$$

where s and s_0 are the unfrozen soil moisture content and the optimum soil moisture, both expressed as a fraction of saturation. $s_0 = 0.5(1 + s_w)$, and $s_{\text{min}} = 1.7s_w$ where s_w is the soil

moisture at wilting point also as a fraction of saturation. The unfrozen soil moisture reduces in the winter and hence provides some additional constraint on the temperature response of soil respiration.

F_v is a function of the vegetation fraction, v :

$$F_v(v) = 0.6 + 0.4(1 - v). \quad (9)$$

All of these modifying functions are poorly constrained, and of these the temperature function has the largest impact on the simulation (Bauer et al., 2008; Exbrayat et al., 2013). Therefore both versions of F_T are evaluated in our simulations.

2.2.2 Vertical discretization

In the new, vertically discretized version of the soil carbon model there is a set of the four soil carbon pools (DPM, RPM, BIO, HUM) in every soil layer. The respiration rate is determined for each soil layer depending on the temperature and moisture conditions in that layer. Following Koven et al. (2013) we also add a vertical mixing (diffusion) term, with diffusivity $D(z)$ in $\text{m}^2 \text{s}^{-1}$ (z is the vertical dimension in m). The equations for each soil carbon pool become

$$\begin{aligned} \frac{\partial C_{\text{DPM}}(z)}{\partial t} &= \frac{\partial}{\partial z} \left(D(z) \frac{\partial C_{\text{DPM}}(z)}{\partial z} \right) \\ &+ f_{\text{dpm}} \Lambda_c(z) - R_{\text{DPM}}(z), \end{aligned} \quad (10)$$

$$\begin{aligned} \frac{\partial C_{\text{RPM}}(z)}{\partial t} &= \frac{\partial}{\partial z} \left(D(z) \frac{\partial C_{\text{RPM}}(z)}{\partial z} \right) \\ &+ (1 - f_{\text{dpm}}) \Lambda_c(z) - R_{\text{RPM}}(z), \end{aligned} \quad (11)$$

$$\begin{aligned} \frac{\partial C_{\text{BIO}}(z)}{\partial t} &= \frac{\partial}{\partial z} \left(D(z) \frac{\partial C_{\text{BIO}}(z)}{\partial z} \right) \\ &+ 0.46\beta_R R_{\text{tot}}(z) - R_{\text{BIO}}(z), \end{aligned} \quad (12)$$

$$\begin{aligned} \frac{\partial C_{\text{HUM}}(z)}{\partial t} &= \frac{\partial}{\partial z} \left(D(z) \frac{\partial C_{\text{HUM}}(z)}{\partial z} \right) \\ &+ 0.54\beta_R R_{\text{tot}}(z) - R_{\text{HUM}}(z). \end{aligned} \quad (13)$$

It is assumed that once respired, any carbon is instantly available to the atmosphere. Both f_{dpm} (the fraction of litter that goes into DPM) and β_R (the fraction of soil respiration emitted to the atmosphere) remain independent of depth. However, the litter inputs, $\Lambda_c(z)$, now vary with depth. In reality, most of the litter enters at the top of the soil, but there is a smaller amount of litter input into deeper soil layers, for example from roots. In JULES, following Koven et al. (2013), we distribute the litter inputs declining exponentially with depth.

We modified the respiration terms in the new model version (from the original, Eq. 5), by including an extra reduction of respiration with depth, based on Jenkinson and Coleman (2008) and Koven et al. (2013). This accounts for factors that are currently missing in the model such as priming

effects, anoxia, soil mineral surface and aggregate stabilization. The respiration terms are now a function of depth as is the total respiration $R_{\text{tot}}(z)$:

$$R_i(z) = k_i C_i(z) F_T(T_{\text{soil}}(z)) F_s(s(z)) F_v(v) \exp(-\tau_{\text{resp}} z). \quad (14)$$

$F_T(T_{\text{soil}}(z))$, $F_s(s(z))$ and $C_i(z)$ are now all dependent on depth. $T_{\text{soil}}(z)$ and $s(z)$ are the simulated layered soil temperature and soil moisture content and $C_i(z)$ is the simulated soil carbon content for each layer and pool i . The respiration is assumed to additionally reduce exponentially with depth and τ_{resp} is an empirical parameter (in m^{-1}) which controls the amount of this reduction. The larger the value of τ_{resp} , the more inhibited the respiration is with increasing depth. In an equilibrium version of the vertically discretized soil carbon model, it was shown that the soil carbon vertical distribution and total amount is strongly dependent on the value of τ_{resp} , more so than any other model parameter.

Since the transport of the respired soil carbon is not yet included in the model, it is assumed that, once respired, the carbon is instantly transferred to the atmosphere. Given that the soil carbon is assumed to be emitted as CO_2 rather than CH_4 , including gas transport processes are unlikely to change the amount emitted but might change the timing of emissions.

The vertical mixing term in Eqs. (10)–(13) represents either bioturbation – mixing of the soil due to animals and plant roots – or cryoturbation – where soil mixing occurs due to frost heave and freeze–thaw processes. The diffusion coefficient, $D(z)$, varies between grid cells and with depth. We follow Koven et al. (2013) by changing the coefficient depending on the presence of permafrost. Without permafrost, there is a bioturbation mixing rate of $1 \text{ cm}^2 \text{ year}^{-1}$. This is constant with depth. When permafrost is present, the mixing represents cryoturbation and the rate increases to $5 \text{ cm}^2 \text{ year}^{-1}$, but drops off linearly below 1 m and reaches zero at 3 m depth (Eq. 15)

$$D(z) = \begin{cases} D_o & ; & z \leq 1 \text{ m} \\ \frac{D_o}{2}(3-z) & ; & 1 \text{ m} < z < 3 \text{ m} \\ 0.0 & ; & z \geq 3 \text{ m} \end{cases} \quad (15)$$

D_o is $5 \text{ cm}^2 \text{ year}^{-1}$. Permafrost is diagnosed wherever the deepest soil layer is below 0°C , assuming that this layer is below the depth of zero annual amplitude. Further modifications to these coefficients could be considered in future work. For example, bioturbation rates may vary with depth (Johnson et al., 2014). There are few explicit measurements of cryoturbation rates, but the available observations suggest that $5 \text{ cm}^2 \text{ year}^{-1}$ may be a realistic value (Klaminder et al., 2014). However, additional studies are required to better constrain soil mixing processes. Some modelling studies have incorporated depth-dependent bioturbation mixing, e.g. Van-walleghem et al. (2013), and there are a few detailed models of cryoturbation, e.g. Peterson et al. (2003).

The soil carbon and soil respiration do not currently feed-back onto any of the land surface processes within JULES.

2.2.3 Adding a soil carbon tracer

In order to more explicitly study soil carbon dynamics in transient simulations, we added a tracer to the model. This works by labelling some of the carbon at the start of the simulation and keeping track of the labels at this carbon moves through the system, whether mixing into different layers or leaving the soil through respiration.

Each soil carbon pool in each soil layer is assigned a fraction, Fr_{oldC} , at the start of the main run, representing the fraction of carbon in that pool that is “labelled”. This fraction is then updated whenever the soil carbon pools are updated, either due to input of fresh carbon from litter (which reduces the fraction), or due to mixing of carbon between two layers in which the fractions are different. The general formula to update the old carbon fraction (Fr_{oldC}) for carbon pool C_i (kg m^{-2}), with an increment of carbon $C_i \rightarrow C_i + \Delta C_i$ is

$$Fr_{\text{oldC}|C_i} \rightarrow \frac{Fr_{\text{oldC}|C_i} C_i + Fr_{\text{oldC}|\Delta C_i} \Delta C_i}{C_i + \Delta C_i}. \quad (16)$$

ΔC_i includes both incoming and outgoing fluxes from the pool. For the outgoing fluxes in ΔC_i , we assume that Fr_{oldC} is the same as for the C_i pool. For an incoming litter flux we assume that Fr_{oldC} is zero, and incoming fluxes from other pools naturally take the Fr_{oldC} value from the corresponding pool. The fraction of labelled carbon in the outgoing respiration flux is also output from the model. This respired “old” carbon is assumed to be instantly transferred to the atmosphere.

Multiplying the carbon pools/fluxes by their corresponding fraction, Fr_{oldC} , gives the quantity of labelled carbon in the pool/flux, allowing the user to follow it through the system.

The choice of which carbon is labelled and traced through the system depends on the scientific question. For example, any carbon that is in permanently frozen soil may be given a value $Fr_{\text{oldC}} = 1$ at the beginning of the simulation, and carbon in other parts of the soil given a value $Fr_{\text{oldC}} = 0$, allowing us to explicitly trace the permafrost carbon. In this paper we label all carbon below 1.0 m with a value of 1 to study the behaviour of the deep soil carbon.

2.3 JULES simulations

Global simulations were carried out using a permafrost version of JULES 4.3 (JULES vn4.3_permafrost). This included the changes to the physical model described by Chadburn et al. (2015a, b). Developments include a representation of moss and organic soils and the addition of bedrock. In addition there was a higher resolution soil column with deeper soil. These modifications result in a reduction in the annual cycle of soil temperatures and a reduction in the summer

thaw depth so that it better matches the observations over the standard configuration of JULES (vn4.3).

The simulations discussed here followed the protocol for the S3 experiments in TRENDY (Sitch et al., 2015). Forcing consisted of time-varying CO₂, climate from the CRU-NCEP data set (v4, 1901–2012), and the fraction of agriculture in each grid cell (Hurtt et al., 2011). The model resolution was N96 (1.875° longitude × 1.25° latitude). Nine plant functional types (PFTs) were used: tropical broadleaf evergreen trees (BET-Tr), temperate broadleaf evergreen trees (BET-Te), broadleaf deciduous trees (BDT), needleleaf evergreen trees (NET), needleleaf deciduous trees (NDT), C3 and C4 grass, evergreen shrubs (ESh), and deciduous shrubs (DSh). These were parametrized following Harper et al. (2016). Plant competition was allowed, with TRIFFID updating vegetation fractions on a daily time step.

Two different model simulations were carried out using the two alternative parametrizations of the soil respiration. The first one is denoted JULES-Q10 and uses $F_{T,Q10}$ (Eq. 6), and $\tau_{\text{resp}} = 2$. The second one is denoted JULES-Roth and uses $F_{T,\text{Roth}}$ (Eq. 7), and $\tau_{\text{resp}} = 1.2$. Respiration is more suppressed at depth in JULES-Q10 than in JULES-Roth. For comparison purposes, additional JULES simulations were carried out using the standard soil carbon model (vn4.3), which uses the temperature and soil moisture from the first layer of the soil to calculate one set of soil carbon pools representative of the whole soil profile. These standard simulations are denoted JULES-Q10_{onelyr} and JULES-Roth_{onelyr}.

The soil carbon distribution is the slowest part of JULES to reach equilibrium. The “modified accelerated decomposition” technique (modified-AD) described by Koven et al. (2013) was used to spin it up to an initial distribution applicable for the year 1900. For the modified-AD the decay rates for the four pools were set to that of the fastest pool. These same factors were used as multipliers to accelerate the diffusion coefficients. An initial equilibrium spin-up of 500 years was carried out to get the vegetation distribution and soil physical properties approximately correct. The model was then spun up by repeating the climate of 1901–1920 25 times. The decomposition rates and the diffusion coefficients were then reset, the soil carbon pools rescaled by the relevant factors and the model spun up until the change in soil carbon was less than 0.012 % decade⁻¹ globally and 0.005 % decade⁻¹ for the permafrost region.

2.4 Evaluation data sets

The circum-Arctic map of permafrost and ground-ice conditions (Brown et al., 1998) gives a historical permafrost distribution, which can be compared with the permafrost area simulated by the model. It records continuous, discontinuous, sporadic, and isolated permafrost zones, for which the estimated permafrost coverage is 90–100, 50–90, 10–50, and < 10 % respectively. Since the model does not include subgrid-scale information, the simulated extent was com-

pared with the continuous and discontinuous regions on the observed map.

There are no large-scale observations of litter available, but the annual total litter will be approximately the same as the annual total net primary productivity (NPP). Observations of NPP are derived from MODIS data using the MOD17 algorithm (Zhao and Running, 2010). Here we assess the multiannual mean NPP for the period 2000 to 2012. Three notable biomes were identified based on 14 World Wildlife Fund terrestrial regions (Olson et al., 2001; Harper et al., 2016): tundra; boreal and coniferous forest; and tropical forest.

There are two different large-scale observationally based soil organic carbon data sets used for evaluation. The WISE30sec data set (Batjes, 2016) was created using the soil map unit delineations of the broad scale Harmonized World Soil Database, version 1.21, with minor corrections, overlaid by a climate zones map as covariate, and soil property estimates derived from analyses of the ISRIC-WISE soil profile database (Batjes, 2009) for the respective mapped “soil/climate” combinations. This is available for soil layer depths of 0–20, 20–40, 40–60, 60–80, 80–100, 100–150, and 150–200 cm. The Northern Circumpolar Soil Carbon Database Version 2 (NCSCDv2: Hugelius et al., 2014) is more appropriate for the northern high latitudes because it includes more site observations than WISE30sec. It is, however, restricted to the northern high latitudes and has a lower-resolution depth structure. NCSCDv2 consists of spatially extrapolated soil carbon data from more than 1700 soil core samples and gives soil organic carbon for the following depths: 0–30, 0–100, 100–200, and 200–300 cm depth.

The multiannual mean and seasonal cycle of observed soil respiration for the period 2000–2012 was extracted from Hashimoto et al. (2015). Hashimoto et al. (2015) combined a global soil database with a semi-empirical model to scale up the field observations of soil respiration to the global scale and provide a data-oriented estimate of soil respiration.

3 Results

The four different JULES simulations – the two standard simulations (JULES-Q10_{onelyr} and JULES-Roth_{onelyr} – vn4.3) and the two vertically discretized simulations (JULES-Q10 and JULES-Roth – vn4.3_permafrost) – all have the same soil physics and vegetation dynamics. The only differences between the simulations are in the soil carbon and soil respiration, which do not feed back onto any of the other land surface processes when JULES is run “offline” driven by observed meteorology (as here).

Figure 2 shows the JULES simulation of the mean permafrost extent for the period between 1961 and 1990, representative of the time period over which the observations were made. The simulated area is 20.3 million km² and the area of the discontinuous and continuous permafrost calcu-

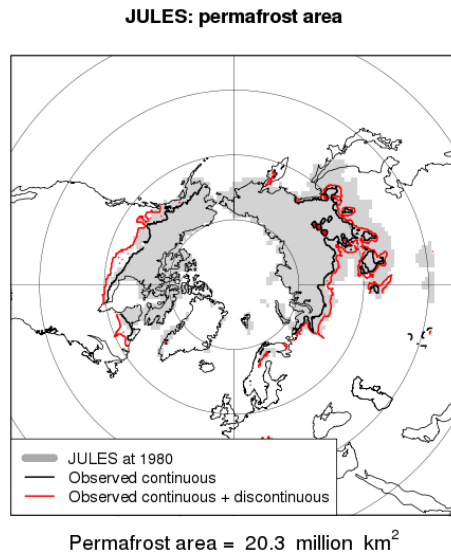


Figure 2. JULES simulated permafrost extent is shaded grey. The boundaries of the observed continuous and discontinuous permafrost are superimposed in black and red.

lated in a similar manner from the Brown et al. (1998) data is 16.5 million km². This slight overestimation by JULES is caused by an overestimation in Eurasia, where the southernmost extent of the simulated permafrost includes regions where there is only isolated or sporadic permafrost, which JULES is not expected to capture.

The addition of the vertical representation of soil carbon is most likely to impact model simulations in the permafrost region, because conditions there are very different in the deeper soil compared with the surface. However, the results must also be assessed both globally and in the tropics to ensure the model remains appropriate for use in a global ESM. Results are presented for three regions: (1) global, (2) tropical (latitudes less than 23.5°), and (3) the region where JULES simulates permafrost and NCSCDv2 has soil carbon data (outlined by a black contour in Fig. 3).

3.1 Soil carbon stocks

The soil carbon quantity and distribution are highly dependent on the surface input of soil organic carbon, which comes from plant litter. Since there are limited observations of litterfall, the simulated NPP was compared with observations (Fig. 3). The large-scale spatial comparison between model and observations is visibly good with a spatial correlation of 0.73. In much of the low and mid-to-high latitudes the simulated NPP is higher than that observed whereas in the drier and colder regions the NPP appears lower. These differences are summarized in Fig. 4. Globally JULES overestimates the annual total NPP by ~12% compared with MODIS. Much of this overestimation occurs in the tropics. In particular, the observed tropical forest biome (right-hand bar plot) is about

a third more productive in JULES than in the observations. In contrast, JULES underestimates the productivity of the permafrost region (highlighted by the black contours in Fig. 3). In general, NPP in the permafrost region is very low – the observed amount is 3.7 Pg C year⁻¹. The JULES-simulated value of 2.5 Pg C year⁻¹ is more than 30% lower than observed. Most of this difference occurs in the observed tundra biome, where the simulated productivity is almost half that of the observations. As with the tropical forest, the boreal forest is slightly too productive, which for the permafrost region as a whole counteracts some of the simulated low-bias from the tundra. Errors in NPP will impact the simulated soil carbon distribution – too low NPP means too little input of organic carbon to the soil, resulting in a low soil carbon whereas too high NPP will cause high soil carbon.

Table 1 shows the total soil carbon simulated by JULES for the different regions and biomes in the top 2 m of the soil. This can be compared with both the WISE30sec data set and the NCSCDv2 data set. In general both of the new vertically discretized JULES models perform better than the standard models when compared with observations. Their global total is more than twice that of the standard model versions and higher than the total in the WISE30sec data set. However, over the NCSCDv2 region the WISE30sec data set has 680 Pg C whilst NCSCDv2 has 1031 Pg C. Therefore WISE30sec simulates 351 Pg C less than NCSCDv2. Roughly combining these two data sets suggests that the global total could be nearer to 2300 Pg and therefore only slightly lower than the new model estimates. The biggest improvement in the vertically resolved model is the amount of soil carbon in the permafrost region. The standard JULES versions (JULES-Roth_{only} and JULES-Q10_{only}) have far too little soil carbon in this region when compared with either the WISE30sec or the NCSCDv2 data. This increases significantly, to a value comparable with the observations, when using JULES-Roth or JULES-Q10. The soil carbon in the cold deep soil takes a long time to reach equilibrium with its amount depending on the balance between the litter input at the surface and the slow soil respiration rate. Once in equilibrium it will not respond notably to short-term climate fluctuations.

In terms of biomes (Table 1), all four versions of the model have a reasonable estimate of the soil carbon in the tropical forest biome. The vertical discretization increases the soil carbon slightly. In the boreal forest biome the soil carbon is slightly lower than observations for the standard version of the model. This increases significantly for the vertically discretized models, leading to an overestimation of the soil carbon in the boreal forest by both model versions. The amount of soil carbon in the tundra is significantly larger for the vertically resolved model versions and closer to both observational data sets, but remains too low. Some of the differences highlighted in Table 1 are caused by errors in the soil carbon input, i.e. NPP (Fig. 4). However, particularly in the cold regions, the errors are also related to missing processes in the

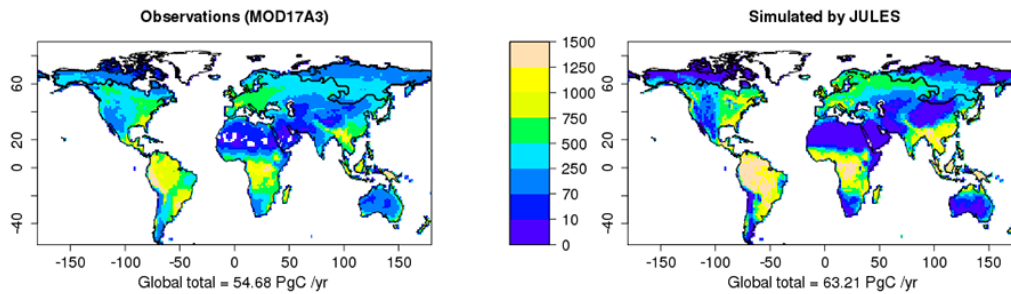


Figure 3. MODIS observed and JULES simulated multiannual mean net primary productivity in $\text{g C m}^{-2} \text{ year}^{-1}$ for the period 2000–2012. The black contours highlight the region where JULES simulates permafrost.

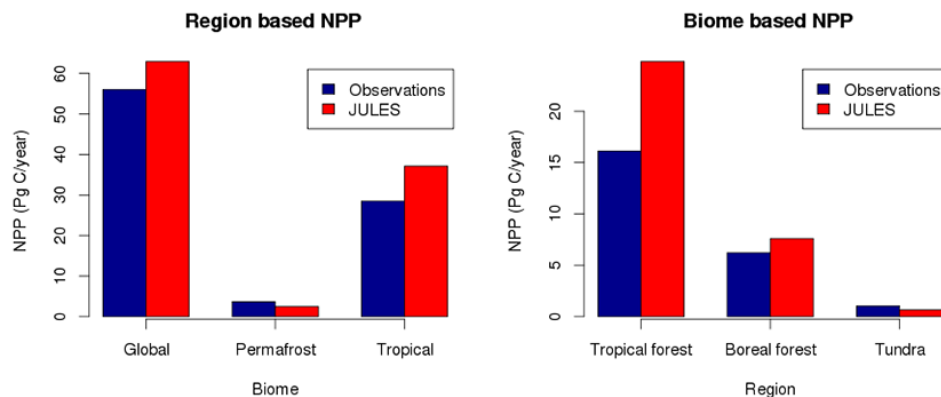


Figure 4. MODIS observed and JULES simulated annual mean NPP for the regions assessed in this paper (left-hand plot), and for the following observed biomes defined by Olson et al. (2001): tropical forest, boreal and coniferous forest, and tundra (right-hand plot). Note the different scales.

model such as dust deposition and peat accumulation. In addition, the observations contain additional soil carbon which is not in equilibrium with the current climate such as peatland and waterlogged soils (Hugelius et al., 2016).

The spatial distribution of the soil carbon in the top 2m of the soil is shown in Fig. 5. On first glance the modelled spatial patterns are very similar, with higher levels of soil carbon in the boreal forest region, eastern America and Europe. Spatial correlations between the standard and layered soil carbon models are high (0.82 between JULES-Roth and JULES-Roth_{only1yr} and 0.92 between JULES-Q10 and JULES-Q10_{only1yr}). However, spatial correlations between the model and WISE30sec observations are lower at 0.40, 0.27, 0.30, and 0.22 for JULES-Roth, JULES-Roth_{only1yr}, JULES-Q10, and JULES-Q10_{only1yr} respectively. There is a slight improvement in the spatial correlation with WISE30sec of the vertically resolved model compared with the standard model, but the values remain relatively low. In comparison with the WISE30sec observations, the model has a greater area in the northern mid-latitudes with high values of soil carbon, and a greater area in the northern high latitudes and deserts with very small amounts of soil carbon. The vertically resolved simulations show more soil carbon in some of these cold regions compared with the standard model, making it more

comparable to the WISE30sec data than the standard simulations. The NCSCDv2 data have much larger amounts of soil carbon in the northern high latitudes than the WISE30sec data, more comparable with the vertically resolved model. This high carbon density extends further north than any of the model simulations.

The two main differences between JULES-Q10 and JULES-Roth are the parametrization of $F_T(T_{\text{soil}})$ and the value of τ_{resp} . The τ_{resp} exerts a strong control over both the total amount of soil carbon present and the vertical distribution of soil carbon within the profile. Respiration is more suppressed at depth in JULES-Q10 ($\tau_{\text{resp}} = 2$) than in JULES-Roth ($\tau_{\text{resp}} = 1.2$) leading to a greater proportion of soil carbon deeper in the soil profile in JULES-Q10 than in JULES-Roth. However τ_{resp} has little impact on the spatial correlations between model and observations. In contrast $F_T(T_{\text{soil}})$ affects the relative amounts of soil carbon in the tropics compared with the polar regions (Fig. 1).

Figure 6 shows the zonal distribution of soil carbon for the permafrost region (highlighted in Fig. 3) for both NCSCDv2 and WISE30sec data. The vertically discretized models are significantly improved over the standard model versions with much more soil carbon at latitudes where the observations show more soil carbon. There is still a mismatch between

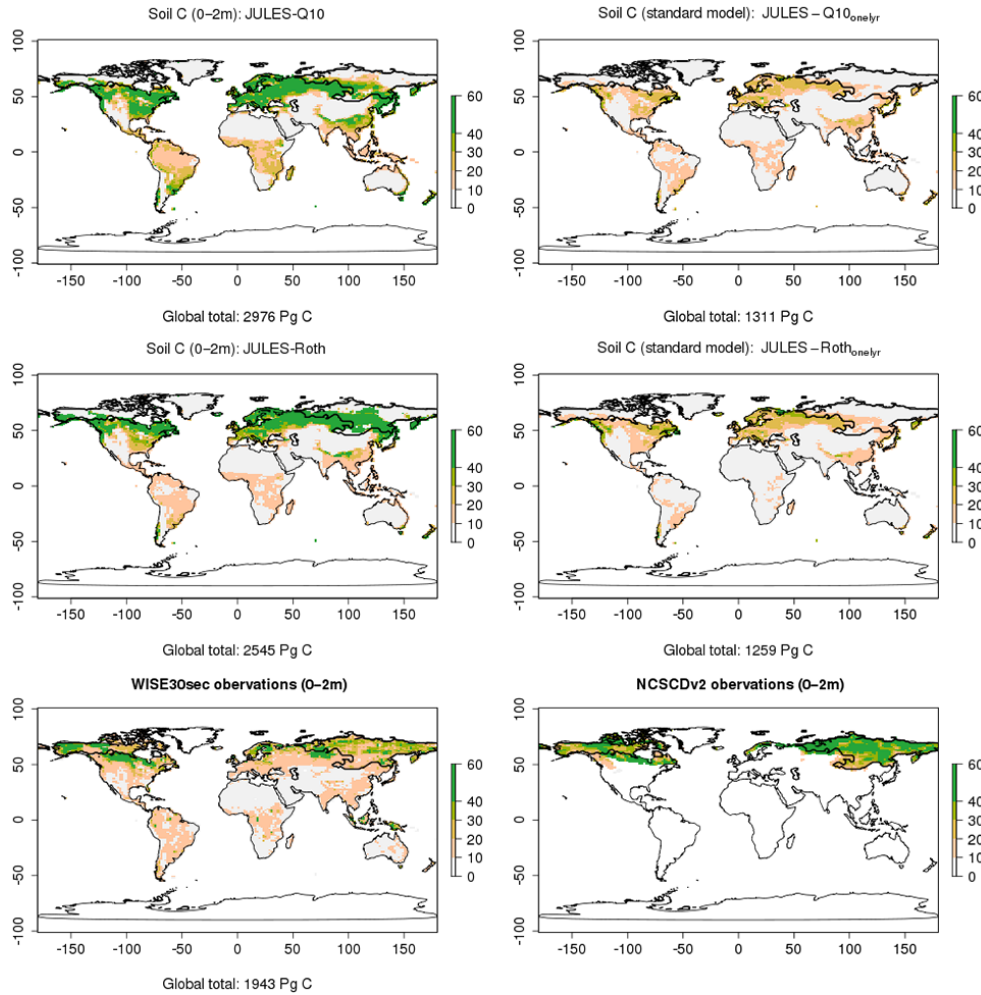


Figure 5. Soil carbon in the top 2 m in kg m^{-2} for the four different model simulations. The new vertically discretized model versions are on the left and the standard model versions are on the right. The WISE30sec observed data set is shown at the bottom left and the NCSCDv2 at the bottom right.

Table 1. Total soil carbon in top 2 m (Pg C) for the regions assessed in this paper (top three lines) and for the following biomes defined by Olson (2001): tropical forest; boreal and coniferous forest; and tundra (bottom three lines). Bold font indicates the vertically discretized soil carbon models.

Region	WISE30sec	NCSCDv2	JULES-Roth	JULES-Roth _{onlyr}	JULES-Q10	JULES-Q10 _{onlyr}
Global	1943		2545	1259	2976	1311
Permafrost	452	741	568	117	325	90
Tropical	542		491	356	832	446
Tropical forest	328		293	218	493	274
Boreal forest	567		959	325	759	275
Tundra	182	292	126	37	72	26

the latitude where the soil carbon is greatest – about 65°N for the observations, but only 60°N for the models. The low simulated soil carbon in the region between 65 and 80°N is partly caused by the low simulated NPP in those regions (Fig. 3).

Figure 7 shows the profile of soil carbon for the regions in this study. The WISE30sec data are only available down to 2 m, whilst the NCSCDv2 is available from 0 to 3 m. In the permafrost region, the WISE30sec and NCSCDv2 have different profiles, with the NCSCDv2 having a greater

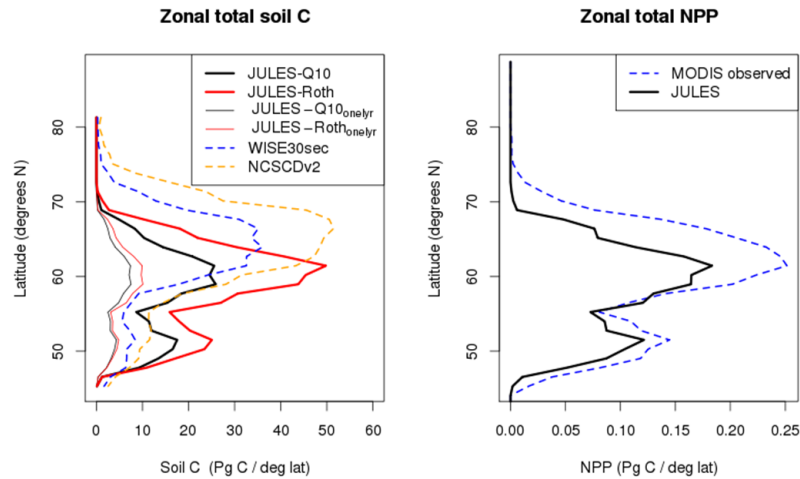


Figure 6. Zonal total of soil carbon (left-hand plot) and NPP (right-hand plot) for the permafrost region highlighted in Fig. 3, expressed as Pg C per degree of latitude.

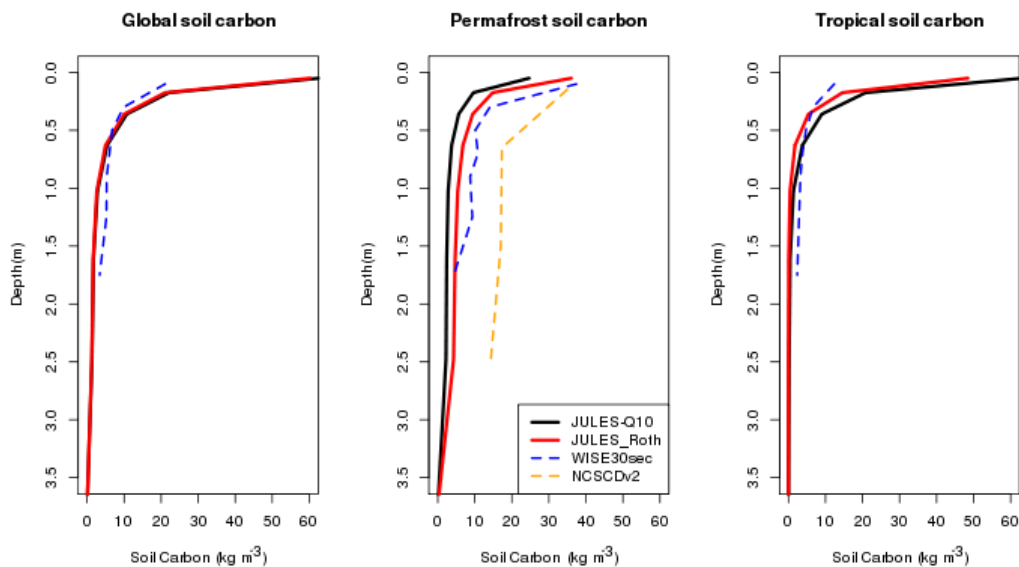


Figure 7. Profile of soil carbon in kg m^{-3} for the three main regions in this study.

proportion of its soil carbon between 1 and 2 m than the WISE30sec data and a smaller proportion nearer the surface. In the modelled permafrost region (highlighted in Fig. 2 in grey) the vertical mixing of the organic carbon through the soil profile represents cryoturbation, whereas for the rest of the global land surface the mixing represents bioturbation, with a smaller mixing rate (see Sect. 2.2.2). The comparison of model and observations suggests that the model simulates too much soil carbon near the surface in the top 50 cm and not enough deeper in the soil both globally and in the tropics, which may be in part due to the representation of bioturbation. In the permafrost region, the model simulations approximately follow the shape of depth distribution of the WISE30sec data, although the soil carbon density is too low.

There are significant differences between the JULES-Roth and JULES-Q10 simulations. The $F_{T,Roth}$ rate-modifying function has a steeper gradient with temperature than the $F_{T,Q10}$ (Fig. 1), meaning that JULES-Roth tends to simulate less soil carbon in warm regions (very high decomposition) and more soil carbon in cold regions (very low decomposition), e.g. Table 1; Fig. 5. These JULES-Roth results overall compare better with the observations, for example in Table 1, Figs. 6 and 7. JULES-Q10 simulates too little soil carbon in the permafrost regions, and globally JULES-Roth has a better spatial correlation with the WISE30sec data (0.4, compared with 0.3 for JULES-Q10).

3.2 Soil respiration

The addition of vertically discretized soil carbon has little impact on the magnitude of the soil respiration (Fig. 8). This is expected because the climate is relatively stable at the beginning of the 21st century and the inputs (litterfall) are expected to approximately equal the outputs (respiration). Figure 8 shows that the seasonal cycle is very similar for all four model versions in the tropics. However, in the permafrost region the seasonal cycle is slightly displaced, so that the peak of the respiration happens later in the year in the vertically resolved simulation. This shifts the peak so that it is approximately 20 days later for both JULES-Q10 and JULES-Roth. In JULES-Q10_{onlyr} and JULES-Roth_{onlyr}, the respiration increases with the warming of the top soil layer in spring and reduces once the soil surface layer cools back down early in the autumn. In JULES-Q10 and JULES-Roth the respiration is dependent on the soil temperature profile – the soil warms up slowly from the surface downwards during late spring leading to a slower increase in respiration as the air temperature increases. At the end of the summer, the deeper soil layers cool more slowly than the surface, so respiration continues for longer. The delay in time of peak respiration is also notable in the total global soil respiration. Including gas transport processes within the soil will further delay the time of peak surface emissions – this process will be included in a later version of JULES.

This change in the seasonal cycle of soil respiration impacts the seasonal cycle of net ecosystem exchange (NEE – Fig. 9). The annual amplitude of the global NEE increases in the vertically resolved models. They uptake more carbon in the Northern Hemisphere spring/summer and lose more in the Northern Hemisphere autumn/early winter. In the permafrost region the onset of carbon uptake is up to a month earlier in the vertically resolved model when compared with the standard model.

JULES-Roth and JULES-Q10 have a different seasonality. JULES-Roth has its peak uptake earlier in the year than JULES-Q10 and begins emitting carbon in August. This emission in August is because the soil respiration in JULES-Roth is higher than the NPP. JULES-Q10 has a smaller seasonal cycle of soil respiration and smaller maximum summer value, resulting in an uptake of carbon for a longer period during the Northern Hemisphere summer. The difference in the annual cycle of soil respiration between JULES-Roth and JULES-Q10 are due to the higher temperature sensitivity of the function $F_{T,Roth}$ compared with $F_{T,Q10}$. The larger seasonal cycle in JULES-Roth is closer to the observed amplitude on Fig. 8.

The changes in the simulated global seasonal cycle of NEE, when included in the Earth system model, will feed-back onto the atmospheric CO₂ and impact any climate simulations.

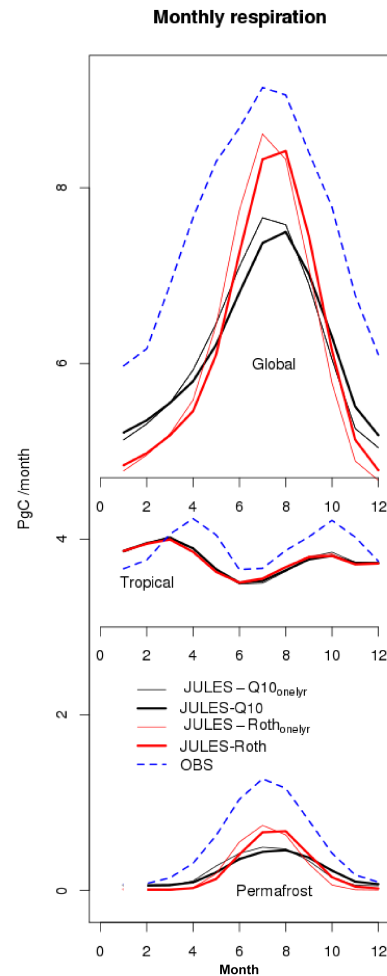


Figure 8. Seasonal cycle of total monthly respiration for the three main regions considered in this paper.

3.3 Soil carbon changes over the 20th century

Figure 10 shows that the inclusion of vertically discretized soil carbon only has a small impact on the change in soil carbon over the 20th century. Globally, the simulated soil carbon increases by around 1 Pg C year^{-1} for the period between 1960 and 2009, with some small differences between model versions. The increase is about $0.15 \text{ Pg C year}^{-1}$ greater for the vertically resolved model than the standard soil carbon model and is a consequence of a slight decrease in the overall sensitivity of soil respiration to temperature changes in the discretized model. The net global response is the combination of an increasing sensitivity of respiration to temperature changes in the warmer regions (tropics – Fig. 10) and a decreasing sensitivity in the colder regions (permafrost – Fig. 10).

In the permafrost region and between 1960 and 2009 the soil carbon increases by 146–168 Tg C. This falls within the modelled spread found by McGuire et al. (2016) who used a range of land surface models and showed the soil

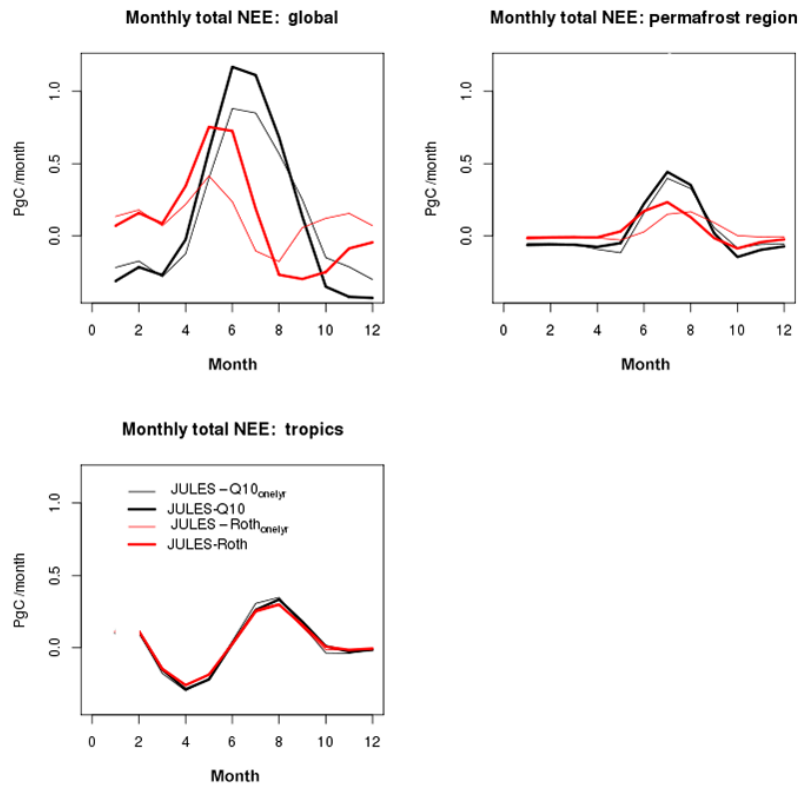


Figure 9. Seasonal cycle of net ecosystem exchange (NEE) for the three main regions considered in this paper. Positive values represent an uptake of carbon and negative values represent a loss of carbon.

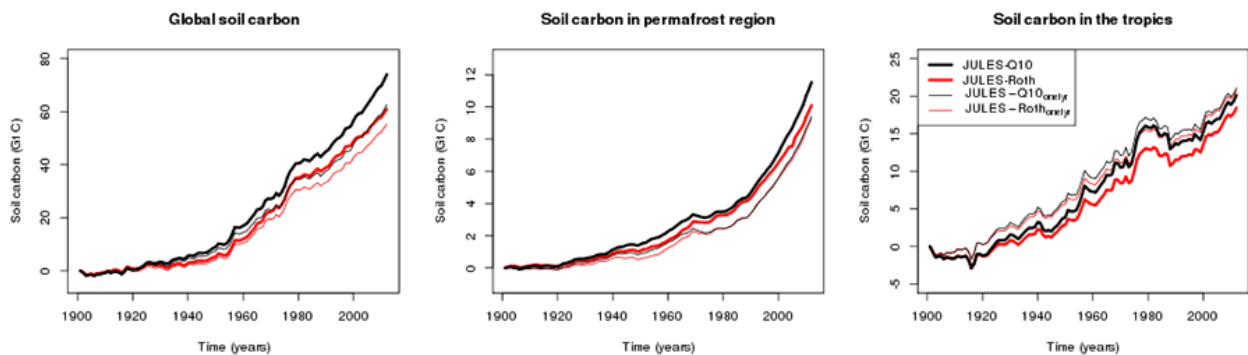


Figure 10. Time series of change in soil carbon (in Pg C) over the 20th century for the three regions: global, permafrost and tropical.

carbon increased over the permafrost region by 264 (42–637) Tg C year⁻¹ for the period 1960–2009. The slightly faster increase (by ~ 10 to 25 Tg C year⁻¹) in the vertically discretized models are a consequence of the lower response of soil respiration to temperature change – possibly caused by a lag in the response of the deep soil temperatures to increasing air temperature. In the standard model, the respiration only responds to the surface soil temperatures, which will respond much more quickly to changes in air temperature than the deeper soil. It should be noted that the difference in the soil carbon between the standard and vertically dis-

cretized model are small compared with differences between different models in, for example, McGuire et al. (2016).

The deep soil carbon was initialized in 1901 and tracked over the 20th century (Fig. 11). Figure 11 shows the spatial distribution of the fraction of the total soil carbon that is labelled as “deep carbon”, i.e. the ratio of the carbon below 1 m depth to the total soil carbon in the profile. In general JULES-Q10 has more deep soil carbon than JULES-Roth because it has more suppression of respiration with depth ($\tau_{\text{resp}} = 2$ compared with $\tau_{\text{resp}} = 1.2$). Both JULES simulations give a large proportion of deep soil carbon in the permafrost re-

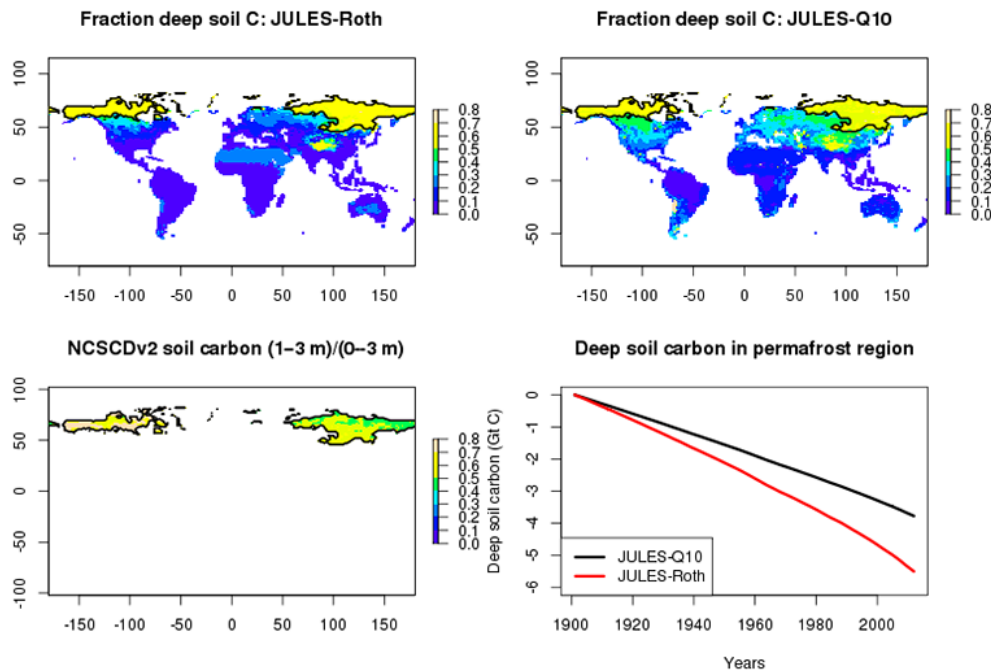


Figure 11. The spatial plots show the deep soil carbon (defined as soil carbon below 1 m in 1901) as a fraction of the total soil carbon for each grid cell. The time series shows the change in labelled deep soil carbon for the permafrost region in Pg C.

Table 2. Labelled deep soil carbon and total soil carbon in the permafrost region before and after adding the NCSCDv2 observed deep soil carbon for depths below 1 m. Any differences between NCSCDv2 and the added labelled deep soil carbon are caused by differences between interpolation methodologies.

Vertically resolved simulations	NCSCDv2	JULES-Roth	JULES-Q10
Mean ratio: deep / total	0.59	0.53	0.60
SD of ratio: deep / total	0.11	0.07	0.06
Total soil carbon (Pg C)	1007	801	446
Labelled deep soil carbon (Pg C)	585	475	251
Added obs. of deep carbon		JULES-Roth	JULES-Q10
Mean ratio: deep / total		0.76	0.81
SD of ratio: deep / total		0.25	0.21
Total soil (Pg C)		855	724
Labelled deep soil carbon (Pg C)		543	528

gions with 53 to 60 % at depths below 1 m (Table 2) and a much lower proportion over the rest of the land surface (particularly for the temperate and tropical regions where it is $\lesssim 20\%$). These proportions are comparable with the proportion observed in the NCSCDv2 data set (59 %), although the absolute magnitude of the soil carbon is too low. However, the observations are much more spatially variable than the model simulations (Table 2 and Fig. 11), with more carbon in the deep soil in North America compared with Eurasia.

The change in the labelled deep soil carbon over the 20th century for the permafrost region highlighted is shown as a time series in Fig. 11. This represents, for example, original permafrost carbon which may be released to the atmo-

sphere in a changing climate (Schuur et al., 2015). Despite an increase in the total soil carbon in the permafrost region (Fig. 10), there is a decrease in the labelled deep soil carbon in the soil profile of around $33\text{--}49\text{ Tg C year}^{-1}$. A further $41\text{--}80\text{ Tg C year}^{-1}$ labelled deep soil carbon is mixed out of the deep soil and into the top 1 m of the soil. Vertical mixing processes in JULES continue to add new deep soil carbon resulting in a net increase in total deep soil carbon of $\sim 100\text{ Tg C year}^{-1}$ over the 20th century. However, this deep soil carbon now consists of both “original” permafrost carbon and “newer” active carbon which, in reality, are likely to have different qualities (Harden et al., 2012). This tracking

of soil carbon could also be used for more detailed model evaluation – see, for example, He et al. (2016).

3.4 Model initialization of permafrost carbon

The new soil carbon model has improved the simulated soil carbon distribution for both versions of JULES. However, there are still considerable errors in the spatial distribution of soil carbon, reflected by the low spatial correlation between model and observations and most notable in the northern polar regions in Figs. 5 and 6. This is caused, in part, by errors in the litter input to the soil – illustrated here as differences between the observed and modelled NPP (Fig. 6). Errors in the litter input are more likely to cause errors in the soil carbon in the active layer which turns over at shorter timescales. Any carbon frozen in the permafrost has been buried over several thousand years by alluvial sedimentation; dust deposition; peat development and cryoturbation (Zimov et al., 2006; Schuur et al., 2008; Ping et al., 2015). The only burial process included in the vertically resolved soil carbon model discussed here is cryoturbation. Therefore the model should not be expected to simulate the soil carbon stores introduced by these additional burial processes. However, errors caused by these missing processes will bias simulations of soil carbon and the response of the soil carbon to a changing climate. This will have implications for any estimate of the permafrost carbon feedback when JULES is used within UKESM.

One method of incorporating a spatially realistic quantity of relatively inert permafrost carbon is to simply replace the simulated deep soil carbon below 1 m with the observed soil carbon from the NCSCDv2 in the permafrost region (“PFC added: JULES-Roth” and “PFC added: JULES-Q10”). JULES has four soil carbon pools, whereas the observations only give total soil carbon. Therefore the observed soil carbon was partitioned into the four pools based on the model’s simulation of partitioning for each grid cell. It was also interpolated to the model soil levels. Table 2 shows that the labelled deep soil carbon in the two JULES simulations is approximately equal to that in the NCSCDv2 data set. This has increased the total soil carbon in the permafrost region so it more closely represents the total observed soil carbon in the NCSDv2. However, there is still a deficit of 122 to 283 Pg C depending on model configuration. The main differences are in the top 1 m of soil, which is simulated by the model. Figure 12 shows the zonal total soil carbon for the permafrost region. The thin red and black lines (“PFC added: JULES-Roth” and “PFC added: JULES-Q10”) show that with the addition of the observed soil carbon below 1 m, JULES is closer to the observations, particularly in the region between 65 and 75° N. The global spatial correlation of the blended model and NCSCDv2 soil carbon with the WISE30sec (top 2 m) increases from 0.40 to 0.53 for JULES-RothC and from 0.3 to 0.43 for JULES-Q10.

The addition of the permafrost carbon to the model could result in a significant drift back towards the equilibrium state.

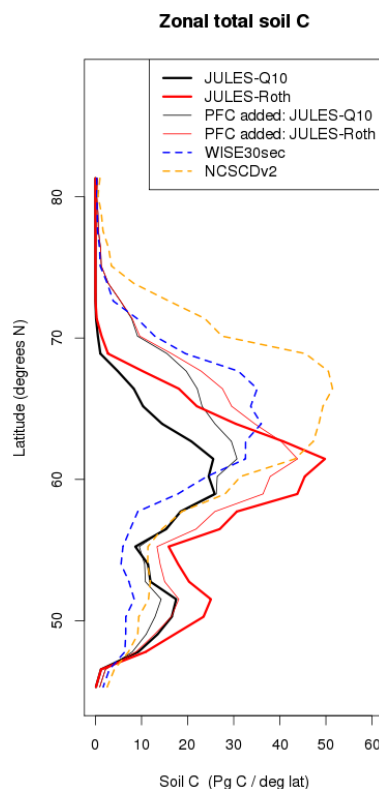


Figure 12. Zonal profile of total soil carbon after re-initialization with observed soil carbon at depths between 1 and 3 m – compared with observations, and with the vertically resolved versions of JULES-Q10 and JULES-Roth.

In order to quantify the size of this drift the model was re-spun up from 1901–1920 for 25×20 years. After 500 years the global soil carbon had increased by 23 Pg C or 0.75 % of the global total for JULES-RothC and decreased by 2 Pg C or 0.06 % for JULES-Q10. The soil carbon in the permafrost region had increased by 7.5 Pg C or 0.9 % of the total in that region for JULES-RothC and decreased by 6.5 Pg C or 0.9 % of the total in that region for JULES-Q10. Figure 13 compares these spin-up simulations with the simulated change in soil carbon over the 20th century, both globally and for the permafrost region. Also shown are two additional 20th century simulations, one made directly after the permafrost carbon was initialized (“20th century climate + permafrost carbon”) and one where the models were re-spun-up for the additional 25×20 years after the permafrost carbon was initialized (“20th century climate + permafrost carbon + further spin-up”). In all cases the change over the 20th century is larger than the trend in the spin-up. For the global simulations, adding the carbon in the permafrost region has little impact on the total simulated change. The very slightly smaller increase in soil carbon is small compared with the differences between the model configurations. In the permafrost region, the overall increase in soil carbon is smaller, and as expected

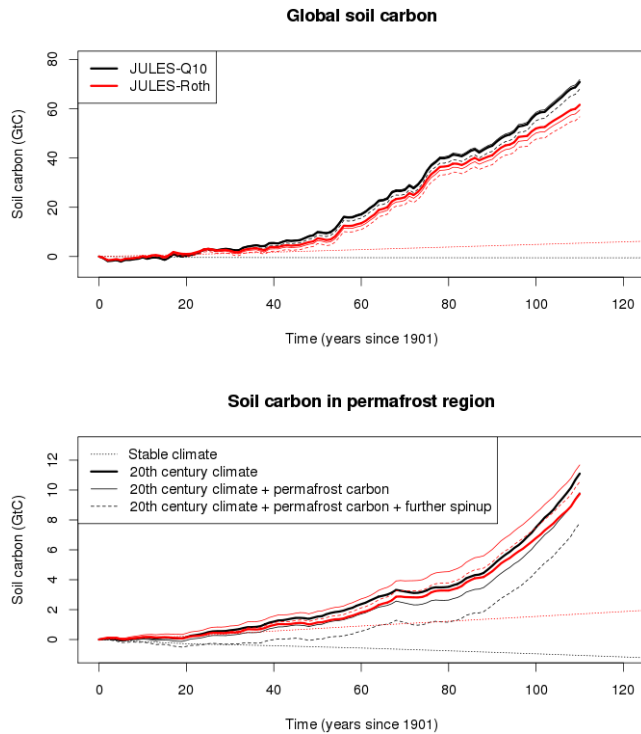


Figure 13. Change in soil carbon over 20th century with and without the observed permafrost carbon added, and with and without further spin-up.

the addition of permafrost carbon has a greater impact on the changes.

4 Conclusions

This paper presents a vertically resolved model of soil carbon developed as a precursor to adding the permafrost carbon feedback into UKESM. This new model includes a tracer so that specified soil carbon (such as permafrost carbon) can be identified, labelled, and followed through the simulation. The vertically resolved model improves the spatial representation of soil carbon when compared to the standard non-vertically resolved model. The seasonal peak of the soil respiration in the Northern Hemisphere summer is delayed by leading to the NEE peaking slightly earlier in the year. Once included within an ESM, the change in seasonal cycle will feed back onto the model simulated climate. The change in soil carbon over the 20th century is comparable with the standard model.

Given the two temperature-dependent rate-modifying functions available in JULES, our results suggest that the RothC temperature function, $F_{T,Roth}$ (Eq. 7), should be used for the vertically discretized version, in preference to the $F_{T,Q10}$ (Eq. 6), as it gives a better match with the observations both for soil carbon distribution and the seasonal cycle of soil respiration. However, there may be some compensating errors due to the incorrect north–south gradient in

NPP. The exact nature of the most relevant soil temperature [$F_T(T_{soil})$] and soil moisture [$F_s(s)$] functions and their applicability across different biomes needs further investigation (Exbrayat et al., 2013). For example, a systematic analysis using a large model ensemble with a range of respiration rate-modifying functions would be very informative.

Two of the most notable remaining sources of model errors are (1) errors in the model simulation of the litter input and (2) missing vertical processes within the soil carbon model such as alluvial sedimentation; dust deposition; peat development. These should all be considered in future model developments. In order to reduce the influence of errors caused by litter, an alternative method of model evaluation may be to use soil carbon turnover times analogous to those used by Carvalhais et al. (2014). These may not be appropriate for simulations of permafrost carbon, but may be useful in determining the behaviour of the soil carbon within the active layer. Hugelius et al. (2016) suggested that the observed carbon stocks could be categorized based on whether the appropriate process is included within an ESM and hence whether the ESM is expected to simulate soil carbon in that region.

Initialization of the deep soil carbon according to the NC-SCDv2 map allowed a better match between the simulated soil carbon and the observed carbon distribution. Although there is a slight drift in the regional and global soil carbon, this is small compared with the change in soil carbon over the 20th century. This methodology may provide a way of initializing an ESM so that the permafrost carbon feedback is more appropriately estimated. However, this then limit the usefulness of the soil carbon observations for model evaluation. Alternative methods of model evaluation need to be developed such as those discussed by He et al. (2016) and Carvalhais et al. (2014).

5 Code availability

The JULES code used in these simulations is available from the Met Office Science Repository Service at https://code.metoffice.gov.uk/trac/jules/browser/main/branches/dev/eleanorburke/vn4.3_permafrost (registration required).

Competing interests. The authors declare that they have no conflict of interest.

Acknowledgements. The authors acknowledge financial support by the European Union FP7-ENVIRONMENT project PAGE21 under contract GA28270 and the European Union Horizon 2020 Project CRESCENDO under contract 641816. Eleanor Burke was supported by the Joint UK BEIS/Defra Met Office Hadley Centre Climate Programme (GA01101). Sarah Chadburn was supported by the Joint Partnership Initiative project COncstraining Uncertainties in the Permafrost-climate feedback (COUP) (National Environment

Research Council grant NE/M01990X/1). We also acknowledge the support of Gustaf Hugelius, who post-processed the WISE30sec data into netcdf form.

Edited by: C. Sierra

Reviewed by: two anonymous referees

References

- Anav, A., Friedlingstein, P., Kidston, M., Bopp, L., Ciais, P., Cox, P., Jones, C., Jung, M., Myneni, R., and Zhu, Z.: Evaluating the Land and Ocean Components of the Global Carbon Cycle in the CMIP5 Earth System Models, *J. Climate*, 26, 6801–6843, doi:10.1175/JCLI-D-12-00417.1, 2013.
- Batjes, N.: Harmonized soil profile data for applications at global and continental scales: updates to the WISE database, *Soil Use Manage.*, 25, 124–127, 2009.
- Batjes, N.: Harmonized soil property values for broad-scale modelling (WISE30sec) with estimates of global soil carbon stocks, *Geoderma*, 269, 61–68, 2016.
- Bauer, J., Herbst, M., Huisman, J., Weihermueller, L., and Vereecken, H.: Sensitivity of simulated soil heterotrophic respiration to temperature and moisture reduction functions, *Geoderma*, 145, 17–27, 2008.
- Best, M. J., Pryor, M., Clark, D. B., Rooney, G. G., Essery, R. L. H., Ménard, C. B., Edwards, J. M., Hendry, M. A., Porson, A., Gedney, N., Mercado, L. M., Sitch, S., Blyth, E., Boucher, O., Cox, P. M., Grimmond, C. S. B., and Harding, R. J.: The Joint UK Land Environment Simulator (JULES), model description – Part 1: Energy and water fluxes, *Geosci. Model Dev.*, 4, 677–699, doi:10.5194/gmd-4-677-2011, 2011.
- Braakhekke, M. C., Beer, C., Hoosbeek, M. R., Reichstein, M., Kruijt, B., Schrupf, M., and Kabat, P.: SOMPROF: A vertically explicit soil organic matter model, *Ecol. Model.*, 222, 1712–1730, doi:10.1016/j.ecolmodel.2011.02.015, 2011.
- Brown, J., Ferrians Jr., O. J., Heginbottom, J., and Melnikov, E.: Circum-arctic map of permafrost and ground ice conditions, National Snow and Ice Data Center, available at: http://nsidc.org/data/docs/fgdc/ggd318_map_circumarctic (last access: 15 February 2017), 1998.
- Burke, E. J., Hartley, I. P., and Jones, C. D.: Uncertainties in the global temperature change caused by carbon release from permafrost thawing, *The Cryosphere*, 6, 1063–1076, doi:10.5194/tc-6-1063-2012, 2012.
- Burke, E. J., Jones, C. D., and Koven, C. D.: Estimating the Permafrost-Carbon Climate Response in the CMIP5 Climate Models Using a Simplified Approach, *J. Climate*, 26, 4897–4909, doi:10.1175/JCLI-D-12-00550.1, 2013.
- Carvalhais, N., Forkel, M., Khomik, M., Bellarby, J., Jung, M., Migliavacca, M., Mu, M., Saatchi, S., Santoro, M., Thurner, M., Weber, U., Ahrens, B., Beer, C., Cescatti, A., Randerson, J., and Reichstein, M.: Global covariation of carbon turnover times with climate in terrestrial ecosystems, *Nature*, 514, 213–217, 2014.
- Chadburn, S., Burke, E., Essery, R., Boike, J., Langer, M., Heikenfeld, M., Cox, P., and Friedlingstein, P.: An improved representation of physical permafrost dynamics in the JULES land-surface model, *Geosci. Model Dev.*, 8, 1493–1508, doi:10.5194/gmd-8-1493-2015, 2015a.
- Chadburn, S. E., Burke, E. J., Essery, R. L. H., Boike, J., Langer, M., Heikenfeld, M., Cox, P. M., and Friedlingstein, P.: Impact of model developments on present and future simulations of permafrost in a global land-surface model, *The Cryosphere*, 9, 1505–1521, doi:10.5194/tc-9-1505-2015, 2015b.
- Clark, D. B., Mercado, L. M., Sitch, S., Jones, C. D., Gedney, N., Best, M. J., Pryor, M., Rooney, G. G., Essery, R. L. H., Blyth, E., Boucher, O., Harding, R. J., Huntingford, C., and Cox, P. M.: The Joint UK Land Environment Simulator (JULES), model description – Part 2: Carbon fluxes and vegetation dynamics, *Geosci. Model Dev.*, 4, 701–722, doi:10.5194/gmd-4-701-2011, 2011.
- Dutta, K., Schuur, E., Neff, J., and Zimov, S.: Potential carbon release from permafrost soils of Northeastern Siberia, *Glob. Change Biol.*, 12, 2336–2351, 2006.
- Ekici, A., Beer, C., Hagemann, S., Boike, J., Langer, M., and Hauck, C.: Simulating high-latitude permafrost regions by the JSBACH terrestrial ecosystem model, *Geosci. Model Dev.*, 7, 631–647, doi:10.5194/gmd-7-631-2014, 2014.
- Exbrayat, J.-F., Pitman, A. J., Zhang, Q., Abramowitz, G., and Wang, Y.-P.: Examining soil carbon uncertainty in a global model: response of microbial decomposition to temperature, moisture and nutrient limitation, *Biogeosciences*, 10, 7095–7108, doi:10.5194/bg-10-7095-2013, 2013.
- Foereid, B., Bellamy, P. H., Holden, A., and Kirk, G. J. D.: On the initialization of soil carbon models and its effects on model predictions for England and Wales, *Eur. J. Soil Sci.*, 63, 32–41, doi:10.1111/j.1365-2389.2011.01407.x, 2012.
- Gouttevin, I., Krinner, G., Ciais, P., Polcher, J., and Legout, C.: Multi-scale validation of a new soil freezing scheme for a land-surface model with physically-based hydrology, *The Cryosphere*, 6, 407–430, doi:10.5194/tc-6-407-2012, 2012.
- Harden, J. W., Koven, C. D., Ping, C.-L., Hugelius, G., David McGuire, A., Camill, P., Jorgenson, T., Kuhry, P., Michaelson, G. J., O'Donnell, J. A., Schuur, E. A. G., Tarnocai, C., Johnson, K., and Grosse, G.: Field information links permafrost carbon to physical vulnerabilities of thawing, *Geophys. Res. Lett.*, 39, L15704, doi:10.1029/2012GL051958, 2012.
- Harper, A. B., Cox, P. M., Friedlingstein, P., Wiltshire, A. J., Jones, C. D., Sitch, S., Mercado, L. M., Groenendijk, M., Robertson, E., Kattge, J., Bönsch, G., Atkin, O. K., Bahn, M., Cornelissen, J., Niinemets, Ü., Onipchenko, V., Peñuelas, J., Poorter, L., Reich, P. B., Soudzilovskaia, N. A., and Bodegom, P. V.: Improved representation of plant functional types and physiology in the Joint UK Land Environment Simulator (JULES v4.2) using plant trait information, *Geosci. Model Dev.*, 9, 2415–2440, doi:10.5194/gmd-9-2415-2016, 2016.
- Hashimoto, S., Carvalhais, N., Ito, A., Migliavacca, M., Nishina, K., and Reichstein, M.: Global spatiotemporal distribution of soil respiration modeled using a global database, *Biogeosciences*, 12, 4121–4132, doi:10.5194/bg-12-4121-2015, 2015.
- He, Y., Trumbore, S. E., Torn, M. S., Harden, J. W., Vaughn, L. J., Allison, S. D., and Randerson, J. T.: Radiocarbon constraints imply reduced carbon uptake by soils during the 21st century, *Science*, 353, 1419–1424, 2016.
- Herbst, M., Hellebrand, H., Bauer, J., Huisman, J., Šimunek, J., Weihermüller, L., Graf, A., Vanderborght, J., and Vereecken, H.: Multiyear heterotrophic soil respiration: Evaluation of a coupled {CO₂} transport and carbon turnover model, *Ecol. Model.*, 214, 271–283, doi:10.1016/j.ecolmodel.2008.02.007, 2008.

- Hugelius, G., Strauss, J., Zubrzycki, S., Harden, J. W., Schuur, E. A. G., Ping, C.-L., Schirmermeister, L., Grosse, G., Michaelson, G. J., Koven, C. D., O'Donnell, J. A., Elberling, B., Mishra, U., Camill, P., Yu, Z., Palmtag, J., and Kuhry, P.: Estimated stocks of circumpolar permafrost carbon with quantified uncertainty ranges and identified data gaps, *Biogeosciences*, 11, 6573–6593, doi:10.5194/bg-11-6573-2014, 2014.
- Hugelius, G., McGuire, A. D., Beer, C., Bohn, T. J., Burke, E. J., Chadburn, S. E., Chen, G., Chen, X., Hayes, D. J., Jafarov, E., Koven, C. D., Peng, S., and Schaefer, K. M.: Comparing permafrost soil carbon pools from earth system models to empirically derived datasets, 20–24 June 2016, XI International Conference on Permafrost, Bibliothek Wissenschaftspark Albert Einstein, Telegrafenberg, Potsdam, Germany, 2016.
- Hurt, G. C., Chini, L. P., Froking, S., Betts, R., Feddema, J., Fischer, G., Fisk, J., Hibbard, K., Houghton, R., Janetos, A., Jones, C. D., Kindermann, G., Kinoshita, T., Klein Goldewijk, K., Rishi, K., Shevliakova, E., Smith, S., Stehfest, E., Thomson, A., Thornton, P., van Vuuren, D. P., and Wang, Y. P.: Harmonization of land-use scenarios for the period 1500–2100: 600 years of global gridded annual land-use transitions, wood harvest, and resulting secondary lands, *Climatic Change*, 109, 117–161, 2011.
- Jafarov, E. and Schaefer, K.: The importance of a surface organic layer in simulating permafrost thermal and carbon dynamics, *The Cryosphere*, 10, 465–475, doi:10.5194/tc-10-465-2016, 2016.
- Jenkinson, D. and Coleman, K.: A model for the turnover of carbon in soil – Model description and windows user guide, Rothamsted Research, Harpenden, UK, 1999.
- Jenkinson, D. S. and Coleman, K.: The turnover of organic carbon in subsoils. Part 2. Modelling carbon turnover, *Eur. J. Soil Sci.*, 59, 400–413, doi:10.1111/j.1365-2389.2008.01026.x, 2008.
- Jenkinson, D. S., Andrew, S. P. S., Lynch, J. M., Goss, M. J., and Tinker, P. B.: The Turnover of Organic Carbon and Nitrogen in Soil [and Discussion], *Philosophical Transactions: Biological Sciences*, 329, 361–368, 1990.
- Johnson, M. O., Mudd, S. M., Pillans, B., Spooner, N. A., Keith Field, L., Kirkby, M. J., and Gloor, M.: Quantifying the rate and depth dependence of bioturbation based on optically-stimulated luminescence (OSL) dates and meteoric ^{10}Be , *Earth Surf. Proc. Land.*, 39, 1188–1196, doi:10.1002/esp.3520, 2014.
- Jones, C. and Sellar, A.: Development of the 1st version of the UK Earth system model, UKESM newsletter no. 1 – August 2015, available at: <http://www.jwcrp.org.uk/research-activity/ukesm-newsarchive.asp> (last access: 15 February 2017), 2015.
- Klaminder, J., Yoo, K., Olid, C., Ramebäck, H., and Vestergaard, A.: Using Short-lived Radionuclides to Estimate Rates of Soil Motion in Frost Boils, *Permafrost Periglac.*, 25, 184–193, doi:10.1002/ppp.1811, 2014.
- Koven, C., Friedlingstein, P., Ciais, P., Khvorostyanov, D., Krinner, G., and Tarnocai, C.: On the formation of high-latitude soil carbon stocks: Effects of cryoturbation and insulation by organic matter in a land surface model, *Geophys. Res. Lett.*, 36, L21501, doi:10.1029/2009GL040150, 2009.
- Koven, C. D., Riley, W. J., Subin, Z. M., Tang, J. Y., Torn, M. S., Collins, W. D., Bonan, G. B., Lawrence, D. M., and Swenson, S. C.: The effect of vertically resolved soil biogeochemistry and alternate soil C and N models on C dynamics of CLM4, *Biogeosciences*, 10, 7109–7131, doi:10.5194/bg-10-7109-2013, 2013.
- Lawrence, D., Slater, A., Romanovsky, V., and Nicolsky, D.: Sensitivity of a model projection of near-surface permafrost degradation to soil column depth and representation of soil organic matter, *J. Geophys. Res.*, 113, F02011, doi:10.1029/2007JF000883, 2008.
- MacDougall, A. H. and Knutti, R.: Projecting the release of carbon from permafrost soils using a perturbed parameter ensemble modelling approach, *Biogeosciences*, 13, 2123–2136, doi:10.5194/bg-13-2123-2016, 2016.
- MacDougall, A. H., Avis, C. A., and Weaver, A. J.: Significant contribution to climate warming from the permafrost carbon feedback, *Nat. Geosci.*, 5, 719–721, doi:10.1038/ngeo1573, 2012.
- McGuire, A. D., Koven, C., Lawrence, D. M., Clein, J. S., Xia, J., Beer, C., Burke, E., Chen, G., Chen, X., Delire, C., Jafarov, E., MacDougall, A. H., Marchenki, S., Nicolsky, D., Peng, S., Rinke, A., Saito, K., Zhang, W., Alkana, R., Bohn, T., Ciais, P., Decharme, B., Ekici, A., Gouttevin, I., Hajima, T., Hayes, D., Ji, D., Krinner, G., Lettenmaier, D., Luo, Y., Miller, P., Moore, J., Romanovsky, R., Schadel, C., Schaefer, K., Schuur, E. A. G., Smith, B., Sueyoshi, T., and Zhuang, Q.: Variability in the sensitivity among model simulations of permafrost and carbon dynamics in the permafrost region between 1960 and 2009, *Global Biogeochem. Cy.*, 30, 1015–1037, 2016.
- Olson, D. M., Dinerstein, E., Wikramanayake, E. D., Burgess, N. D., Powell, G. V., Underwood, E. C., D'Amico, J. A., Itoua, I., Strand, H. E., Morrison, J. C., Loucks, C. J., Allnutt, T. F., Ricketts, T. H., Kura, Y., Lamoreux, J., Wettengel, W. W., Hedao, P., and Kassem, K.: Terrestrial Ecoregions of the World: A New Map of Life on Earth A new global map of terrestrial ecoregions provides an innovative tool for conserving biodiversity, *BioScience*, 51, 933–938, 2001.
- Paquin, J.-P. and Sushama, L.: On the Arctic near-surface permafrost and climate sensitivities to soil and snow model formulations in climate models, *Clim. Dynam.*, 44, 203–228, doi:10.1007/s00382-014-2185-6, 2015.
- Peterson, R., Walker, D., Romanovsky, V., Knudson, J., Raynolds, M., and Krantz, W.: A differential frost heave model: cryoturbation-vegetation interactions, in: *Proceedings of the Eighth International Conference on Permafrost*, Vol. 2, 885–890, University of Zurich, Switzerland, 2003.
- Ping, C. L., Jastrow, J. D., Jorgenson, M. T., Michaelson, G. J., and Shur, Y. L.: Permafrost soils and carbon cycling, *SOIL*, 1, 147–171, doi:10.5194/soil-1-147-2015, 2015.
- Porada, P., Ekici, A., and Beer, C.: Effects of bryophyte and lichen cover on permafrost soil temperature at large scale, *The Cryosphere*, 10, 2291–2315, doi:10.5194/tc-10-2291-2016, 2016.
- Schaefer, K., Lantuit, H., Romanovsky, V. E., Schuur, E. A. G., and Witt, R.: The impact of the permafrost carbon feedback on global climate, *Environ. Res. Lett.*, 9, 085003, doi:10.1088/1748-9326/9/8/085003, 2014.
- Schirmermeister, L., Siegert, C., Kuznetsova, T., Kuzmina, S., Andreev, A., Kienast, F., Meyer, H., and Bobrov, A.: Paleoenvironmental and paleoclimatic records from permafrost deposits in the Arctic region of Northern Siberia, *Quaternary Int.*, 89, 97–118, doi:10.1016/S1040-6182(01)00083-0, 2002.
- Schneider von Deimling, T., Meinshausen, M., Levermann, A., Huber, V., Frieler, K., Lawrence, D. M., and Brovkin, V.: Estimating

- the near-surface permafrost-carbon feedback on global warming, *Biogeosciences*, 9, 649–665, doi:10.5194/bg-9-649-2012, 2012.
- Schneider von Deimling, T., Grosse, G., Strauss, J., Schirrmeyer, L., Morgenstern, A., Schaphoff, S., Meinshausen, M., and Boike, J.: Observation-based modelling of permafrost carbon fluxes with accounting for deep carbon deposits and thermokarst activity, *Biogeosciences*, 12, 3469–3488, doi:10.5194/bg-12-3469-2015, 2015.
- Schuur, E. A., Bockheim, J., Canadell, J. G., Euskirchen, E., Field, C. B., Goryachkin, S. V., Hagemann, S., Kuhry, P., Laffleur, P. M., Lee, H., Mazhitova, G., Nelson, F., Rinke, A., Romanovsky, V., Shiklomanov, N., Tarnocai, C., Venevsky, S., Vogel, J., and Zimov, S.: Vulnerability of permafrost carbon to climate change: implications for the global carbon cycle, *BioScience*, 58, 701–714, 2008.
- Schuur, E. A. G., McGuire, A. D., Schadel, C., Grosse, G., Harden, J. W., Hayes, D. J., Hugelius, G., Koven, C. D., Kuhry, P., Lawrence, D. M., Natali, S. M., Olefeldt, D., Romanovsky, V. E., Schaefer, K., Turetsky, M. R., Treat, C. C., and Vonk, J. E.: Climate change and the permafrost carbon feedback, *Nature*, 520, 171–179, doi:10.1038/nature14338, 2015.
- Shangguan, W., Dai, Y., Duan, Q., Liu, B., and Yuan, H.: A global soil data set for earth system modeling, *Journal of Advances in Modeling Earth Systems*, 6, 249–263, 2014.
- Sitch, S., Friedlingstein, P., Gruber, N., Jones, S. D., Murray-Tortarolo, G., Ahlström, A., Doney, S. C., Graven, H., Heinze, C., Huntingford, C., Levis, S., Levy, P. E., Lomas, M., Poulter, B., Viovy, N., Zaehle, S., Zeng, N., Arneth, A., Bonan, G., Bopp, L., Canadell, J. G., Chevallier, F., Ciais, P., Ellis, R., Gloor, M., Peylin, P., Piao, S. L., Le Quéré, C., Smith, B., Zhu, Z., and Myneni, R.: Recent trends and drivers of regional sources and sinks of carbon dioxide, *Biogeosciences*, 12, 653–679, doi:10.5194/bg-12-653-2015, 2015.
- Smith, L., MacDonald, G., Velichko, A., Beilman, D., Borisova, O., Frey, K., Kremenetski, K., and Sheng, Y.: Siberian peatlands a net carbon sink and global methane source since the early Holocene, *Science*, 303, 353–356, 2004.
- Tian, H., Lu, C., Yang, J., Banger, K., Huntzinger, D. N., Schwalm, C. R., Michalak, A. M., Cook, R., Ciais, P., Hayes, D., Huang, M., Ito, A., Jain, A. K., Lei, H., Mao, J., Pan, S., Post, W. M., Peng, S., Poulter, B., Ren, W., Ricciuto, D., Schaefer, K., Shi, X., Tao, B., Wang, W., Wei, Y., Yang, Q., Zhang, B., and Zeng, N.: Global patterns and controls of soil organic carbon dynamics as simulated by multiple terrestrial biosphere models: Current status and future directions, *Global Biogeochem. Cy.*, 29, 775–792, doi:10.1002/2014GB005021, 2015.
- Todd-Brown, K. E. O., Randerson, J. T., Post, W. M., Hoffman, F. M., Tarnocai, C., Schuur, E. A. G., and Allison, S. D.: Causes of variation in soil carbon simulations from CMIP5 Earth system models and comparison with observations, *Biogeosciences*, 10, 1717–1736, doi:10.5194/bg-10-1717-2013, 2013.
- Vanwalleghem, T., Stockmann, U., Minasny, B., and McBratney, A. B.: A quantitative model for integrating landscape evolution and soil formation, *J. Geophys. Res.-Earth Surf.*, 118, 331–347, doi:10.1029/2011JF002296, 2013.
- Zhao, M. and Running, S. W.: Drought-induced reduction in global terrestrial net primary production from 2000 through 2009, *Science*, 329, 940–943, 2010.
- Zimov, S. A., Davydov, S. P., Zimova, G. M., Davydova, A. I., Schuur, E. A. G., Dutta, K., and Chapin, F. S.: Permafrost carbon: Stock and decomposability of a globally significant carbon pool, *Geophys. Res. Lett.*, 33, 120502, doi:10.1029/2006GL027484, 2006.